communications biology

A Nature Portfolio journal

Article

https://doi.org/10.1038/s42003-025-08236-z

In situ structure and assembly of the ABC-type tripartite pump MacAB-TolC

Tong Huo[1,6], Wenfang Zhang[2,3,6], Zhili Yu[1,6], Wei Zheng[2,3,6], Yaoming Wu[2,3], Qiuyu Ren[2,3], Zekai Wan[2,3], Junli Cao[2,3] ✉, Zhao Wang[1,4,5] ✉ & Xiaodong Shi[2,3] ✉

The MacAB-TolC tripartite efflux pump is widely distributed in Gram-negative bacteria, extruding antibiotics and virulence factors that lead to multidrug resistance and pathogenicity. However, the in situ structure and assembly mechanism of MacAB-TolC remain unclear. Here, we resolve the in situ structures of the MacAB-TolC efflux pump in *Escherichia coli* by electron cryo-tomography and subtomogram averaging. In the cells without antibiotic treatment, we observe a fully assembled MacAB-TolC pump. When *Escherichia coli* cells are treated with erythromycin, in addition to the tripartite pumps, we also discover the emergence of MacA-TolC subcomplexes without MacB, indicating flexible binding of MacB in the presence of an antibiotic substrate, which is further validated by in vivo photo-crosslinking results. Together, our data suggest the in situ assembly process of MacAB-TolC starts from the formation of MacA-TolC subcomplex, and provides insights into the design of efflux pump inhibitors.

The multidrug resistance (MDR) of Gram-negative bacteria has become one of the foremost global public health threats. This resistance renders the inefficacy of commonly used antibiotics, posing an urgent challenge for clinical anti-infection treatment. Within Gram-negative bacteria, the tripartite efflux pumps spanning the cell envelope account for the active expelling of antibiotics and toxic compounds out of the bacterial cells. This process is a significant determinant of bacteria survival under antibiotic pressure, leading to the initiation of MDR[1]. MacAB-TolC represents one of the tripartite efflux systems, comprising the outer membrane protein TolC, the periplasmic adaptor protein MacA, and the inner membrane transporter MacB from the ATP-binding cassette (ABC) superfamily[2]. This pump actively extrudes various substrates, including macrolide antibiotics and virulence factors, thus contributing to both drug resistance and virulence phenotypes in *Escherichia coli* (*E. coli*) and other Gram-negative bacteria[3].

The crystal structures of MacA[4], TolC[5], and MacB[6,7] were all accessible through the Protein Data Bank (PDB). However, there are only in vitro cryo-electron microscopy (cryo-EM) single-particle structures of fusion-stabilized or disulfide bond-stabilized MacAB-TolC pumps due to the difficulty in isolating the native full assembly through the purification procedure[8]. The failure to purify the fully assembled MacAB-TolC indicates low binding affinities among the three components. Furthermore, it is essential to highlight that the assembly process of tripartite pumps requires a cellular environment. All the above make capturing the intermediate states during the assembly of the MacAB-TolC pump in vitro challenging, leaving the assembly mechanism of this pump in living bacteria unclear.

TolC is the outer membrane component of several tripartite efflux pumps. In our previous study on another TolC-containing tripartite pump, AcrAB-TolC, which belongs to the resistance-nodulation-cell division (RND) superfamily, we found that AcrA and AcrB first form a subcomplex and then recruit TolC[9]. This suggested a possible tripartite pump assembly path, in which the periplasmic membrane fusion protein and inner member component of the pump bind to each other first and then recruit the outer membrane component. However, whether all the TolC-containing tripartite pumps are assembled in the same sequence, with TolC being recruited last, is unclear. Besides, previous studies have shown that purified MacA alone can bind TolC[10–13] as well as MacB[10,12,14], suggesting two possible pathways for the MacAB-TolC efflux pump to assemble, but it is not clear which one is actually employed under the cellular condition. Here, by employing electron cryo-tomography (cryo-ET) and subtomogram averaging, we resolve two different in situ structures of the MacAB-TolC efflux pump from *E. coli* cells in the near-to-native state and substrate-present states. Our finding provides insights into the assembly mechanisms of ABC-type tripartite efflux pumps within their physiological cellular environment.

[1]Verna and Marrs McLean Department of Biochemistry and Molecular Pharmacology, Baylor College of Medicine, Houston, TX, USA. [2]Jiangsu Province Key Laboratory of Anesthesiology and Jiangsu Province Key Laboratory of Anesthesia and Analgesia Application, Xuzhou Medical University, Xuzhou, China. [3]National Medical Products Administration Key Laboratory for Research and Evaluation of Narcotic and Psychotropic Drugs, Xuzhou Medical University, Xuzhou, China. [4]CryoEM/ET core, Baylor College of Medicine, Houston, TX, USA. [5]Department of Molecular and Cellular Biology, Baylor College of Medicine, Houston, TX, USA. [6]These authors contributed equally: Tong Huo, Wenfang Zhang, Zhili Yu, Wei Zheng. ✉e-mail: caojl0310@aliyun.com; zhaow@bcm.edu; shixd@xzhmu.edu.cn

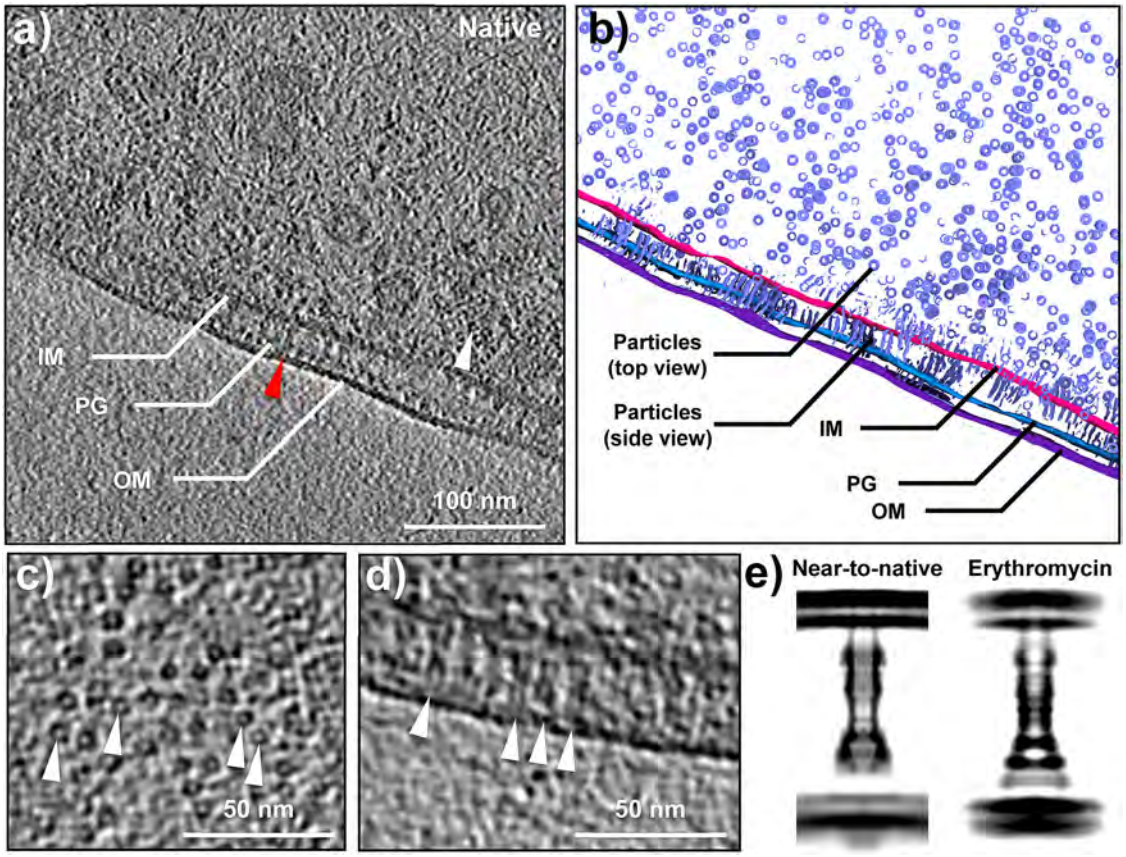

Fig. 1 | Visualization of the MacAB-TolC pump in the near-to-native *E. coli* cell envelope. a A single Z slice from a tomogram of an *E. coli* cell expressing MacA, MacB, and TolC. The side view and top view of MacAB-TolC particles are indicated by the red arrowhead and the white arrowhead, respectively. **b** A tomogram segmentation of (**a**). All Z slices are shown, including particles in all Z levels within this tomogram. The particle side views are within the cell envelope, while particle top views are located at the top and bottom surface of this cell. **c** Zoomed-in view of the MacAB-TolC top view particles (indicated by white arrowheads). **d** Zoomed-in view of the MacAB-TolC side view particles (indicated by white arrowheads). **e** The 2D projection of the rotationally averaged density map of the in situ structure of MacAB-TolC in the near-to-native (left) and erythromycin-treated (right) *E. coli* cells. IM inner membrane, OM outer membrane, PG peptidoglycan.

Results

Visualization of MacAB-TolC pumps in the *E. coli* cell envelope

To visualize MacAB-TolC pumps in the *E. coli* cell envelope, we adopted the same strategy as our previous efflux pump studies[9,15] to augment the in situ MacAB-TolC concentration (Supplementary Fig. 1). Briefly, we overexpressed MacA, MacB, and TolC in BL21(DE3) cells at a level at which the cells can still replicate and grow. Next, we used cryo-ET to directly image the cells without antibiotic treatment. We selected the intact cells with continuous cell envelopes for cryo-ET data collection. In total, 70 tilt series were collected using a 300-kV microscope. The three-dimensional (3D) tomographic reconstruction shows that the bacterial envelope has numerous channel-like densities spanning through, indicating the presence of assembled MacAB-TolC (Fig. 1). The visualization and following segmentation and labeling of the reconstructed densities present a uniform particle size, and the contrast of the image is consistent with our previous studies of the AcrAB-TolC tripartite pump in bacteria[9,15]. We also observed that the distance between the inner and outer membranes remained constant at the locations where the MacAB-TolC pumps occurred, implying that these assemblies may be constricting the periplasm (Fig. 1a, b, d). In the tomograms, the densities of top-view particles appear as discernible circular features (Fig. 1c). When viewed from the side, the particles appear as paired lines connecting the inner and outer membranes and spanning the entire cell envelope (Fig. 1d).

In situ structure of the fully assembled MacAB–TolC complex

For subtomogram averaging of the near-to-native state MacAB-TolC, 5183 particles were used, and the final refinement achieved a resolution of 14 Å (Supplementary Fig. 2). The MacAB-TolC structure (PDB: 5NIK) was docked into the map, with the overall shape of MacB, MacA, and TolC structures well-fitted with the map. The density for the outer and inner membrane observed in this study is located at the TolC β-barrel domain and the MacB transmembrane domain, respectively, indicating that the MacAB-TolC pump spans the full periplasm (Fig. 2a). The interior of the density corresponding to TolC viewed in a cross-section through the averaged map did not have any constriction site at the interface between MacA and TolC, which made TolC a fully open tunnel to the top of the outer membrane (Fig. 2a). In contrast, we observed within the density corresponding to MacA a weak constriction sealing the pump channel (Fig. 2a), the position of which corresponds to the gating ring of MacA[8]. This indicates that MacA resembles a closed state under this experimental condition. The periplasmic domain (PLD) of MacB could be identified, which forms interactions with MacA. The nucleotide binding domain (NBD) of MacB, which was proposed by Fitzpatrick et al.[8], could also be visualized, indicating the presence of the MacB cytoplasmic part (Fig. 2a). Notably, although we did not observe low occupancy in the TolC region or MacB region in the density map of MacAB-TolC, we still performed focused classification. This classification yielded only one map of the fully assembled pump, indicating that neither the MacA-MacB subcomplex nor the MacA-TolC subcomplex exists.

Erythromycin facilitates the detaching of MacB from MacAB-TolC

To understand pump structural response under antibiotic pressure, we treated the MacAB-TolC-overexpressing *E. coli* cells with erythromycin and followed the same imaging pipeline as mentioned above. Erythromycin is

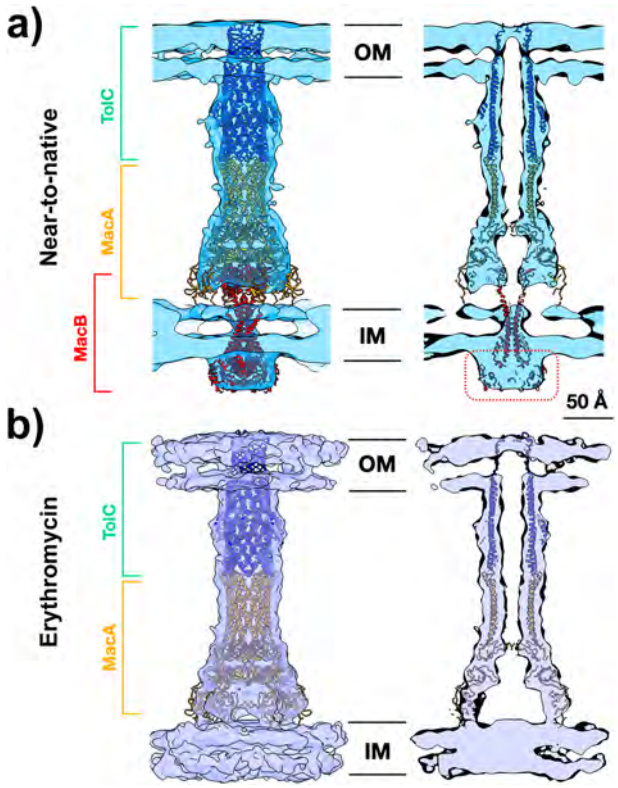

Fig. 2 | In situ cryo-ET structures of the assembled MacAB-TolC complex and MacA-TolC subcomplex. a Density maps of MacAB-TolC in the near-to-native state fitted with the high-resolution MacAB-TolC cryo-EM model (PDB: 5NIK), and its central cross-section view. **b** MacA-TolC under erythromycin pressure fitted with the high-resolution MacAB-TolC (MacB-omitted) cryo-EM model (PDB: 5NIK), and its central cross-section view. The positions of each component of the MacAB-TolC complex and the MacA-TolC subcomplex were determined by comparing with the high resolution MacAB-TolC PDB map. The red dashed line box denotes the NBD of MacB. IM inner membrane, OM outer membrane.

the main substrate of MacAB-TolC and a representative of the macrolide antibiotics[12], which is one of the commonly used antibiotics in clinical treatment[16]. Except for the treatment by erythromycin, all the other experimental processes are the same as those for near-to-native state MacAB-TolC. We carried out minimum inhibitory concentration (MIC) experiments in the strains with both the *acrA* and *acrB* genes knocked out, and the results demonstrated that the MacAB-TolC expressed by the plasmids we constructed was functional (Supplementary Fig. 3 and Supplementary Data 1). The feature of 3D tomographic reconstruction resembles that of MacAB-TolC-overexpressing *E. coli* cells without erythromycin treatment (Supplementary Fig. 4). However, the initial refinement shows that the density at the MacB region is weak compared to MacA and TolC in the complex, suggesting an occupancy variation in the dataset. While in the apo dataset, we did not observe such low occupancy. After focused classification and further refinement of the particles, we obtained a density map showing an absence in the MacB region, with the PLD domain being invisible (Fig. 1e). Subsequently, we resolved the structure of the MacA-TolC subcomplex at around 12 Å (Supplementary Fig. 2) and found that the structure is consistent with the counterpart of that in the MacAB-TolC pump. Missing MacB resulted in the formation of an empty chamber between the MacA membrane-proximal (MP) domains and the inner membrane (Fig. 2b). To rule out the possibility that the appearance of MacA-TolC subcomplexes is due to the decreased expression of MacB after treatment with erythromycin, we performed immunoblotting analysis of the MacB level in the *E. coli* BL21(DE3) cells used for in situ structural studies. As shown in the Supplementary Fig. 5 (Supplementary Data 2), erythromycin had no effect on the expression of MacB ($p = 0.8543$, $R^2 = 0.0095$), but erythromycin indeed caused a weak density in the MacB region. Taken together, these results suggest that erythromycin, as a substrate of MacAB-TolC, facilitates MacB's detachment from the pump complex in cells.

Based on this result, we further validated whether MacA and TolC could form a stable complex on the cell envelope without MacB. We overexpressed MacA and TolC but not MacB in *E. coli* cells and prepared the cryo-ET specimen using the same strategy. We collected 67 tilt series and performed tomogram reconstruction. Within the tomograms, we could observe pump-like features across the cell envelope, indicating the existence of the MacA-TolC subcomplex (Supplementary Fig. 6). This observation confirmed that MacA and TolC can bind to each other without MacB and form a complex on the cell envelope, which indicates that the MacA-TolC subcomplex can exist as a stable entity in cells. We have attempted to perform subtomogram averaging for the MacA-TolC dataset, but it did not yield a well-converged density map. This indicates that in situ MacA-TolC subcomplexes may exist in multiple conformations in the absence of MacB.

In vivo photo-crosslinking results support the detaching of MacB from MacAB-TolC upon erythromycin treatment

To further investigate whether erythromycin facilitates the detaching of MacB from MacAB-TolC, we performed site-specific photo-crosslinking mediated by *p*-benzoyl-L-phenylalanine (Bpa) to determine the interactions between MacA and MacB within cells. Site-specific photo-crosslinking is an effective method for studying the dynamic interactions of proteins in vivo. Recently, it has been successfully used to study the interactions between the LolCDE complex, a member of the ABC transporter family, and lipoproteins[17]. Based on the existing structure (PDB: 5NIK and 5LIL), four amino acid sites at the MacA-MacB interaction region were chosen for Bpa substitution. These sites include Proline 430 (P430) and Leucine 495 (L495) on the MacB, as well as Threonine 53 (T53) and Valine 269 (V269) on the MacA (Fig. 3a). According to the interaction data calculated by CCP4[18], these four residues keep participating in the interaction between MacA and MacB, regardless of whether MacB is in an ATP-bound state or nucleotide-free state (Supplementary Fig. 7 and Supplementary Table 1). As displayed in Supplementary Figs. 8 and 9, Bpa was successfully incorporated into the selected position of target proteins. Through MIC assay, we confirmed that the function of the MacAB-TolC pump was barely affected by Bpa substitution (Supplementary Table 2, Supplementary Fig. 10, and Supplementary Data 3). When the *E. coli* cells expressing MacB Bpa variants and MacA, or MacA Bpa variants and MacB, were subjected to UV radiation, obvious MacA-MacB complexes (as indicated by asterisks in Fig. 3b, c) were detected with MacB Bpa substitutions of L495, and MacA Bpa substitutions of V269, while in the crosslinking products of the cells expressing wild-type MacAB/MacB, as well as the cells expressing the MacB Bpa variants alone, no such complexes were detected (Fig. 3b, c). After identifying the bands that correspond to the MacA-MacB complexes, we evaluated the impact of erythromycin treatment on these complexes in *E. coli* cells. Compared with the control group, after treatment with erythromycin, the MacA-MacB complexes crosslinked by $MacB^{L495Bpa}$ and $MacA^{V269Bpa}$ decreased significantly (for $MacB^{L495Bpa}$, $p = 0.0045$, $R^2 = 0.9376$; for $MacA^{V269Bpa}$, $p = 0.0093$, $R^2 = 0.8873$) (Fig. 3d, e and Supplementary Data 4). Taken together, our in vivo protein photo-crosslinking data indicate that the interaction between MacA and MacB was reduced upon erythromycin treatment, supporting the structural result that MacB exhibits flexible binding behavior in the MacAB-TolC complex in the presence of erythromycin.

Discussion

In this study, we show the in situ structures of the MacAB-TolC efflux pump in *E. coli*, both in near-to-native and erythromycin-present states. In the near-to-native state, we only observed the MacAB-TolC complexes; in the erythromycin-present states, MacAB-TolC complexes became less abundant, and MacA-TolC subcomplexes emerged. Besides, we confirmed that intracellular MacA-TolC subcomplexes exist in the absence of MacB, but in

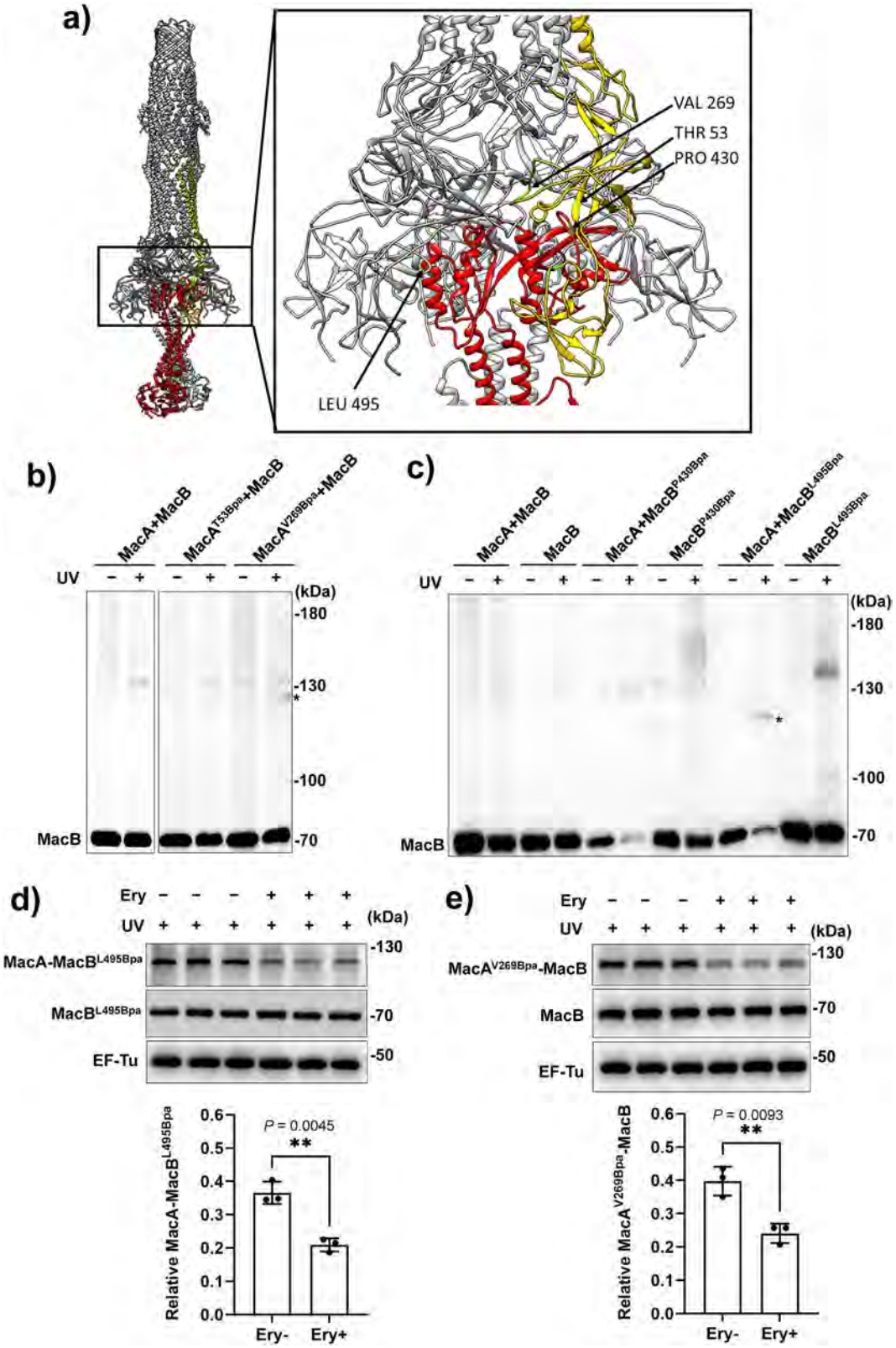

Fig. 3 | The in vivo photo-crosslinked products corresponding to MacA-MacB complexes of MacA/MacB Bpa variants were significantly reduced after erythromycin treatment. a The positions of introduced Bpa in MacA and MacB are shown by black arrows in the MacAB-TolC cryo-EM model (PDB: 5NIK). **b**, **c** Immunoblotting results of the in vivo photo-crosslinked products of the MacA/MacB Bpa variants. The cells expressing indicated proteins were irradiated for 10 min and analyzed by anti-His tag antibodies. The bands representing MacA-MacB complexes were indicated by black asterisks. All immunoblotting results were determined at least three times independently with similar results. **d**, **e** Erythromycin treatment reduced the formation of MacA-MacB complexes in vivo. The cells expressing MacA, MacB^{L495Bpa}, and TolC, and the cells expressing MacA^{V269Bpa}, MacB, and TolC were treated at OD_{600} of 1 with 40 μg/ml erythromycin, respectively. After that, cells were irradiated by UV for 20 min and analyzed by anti-his tag antibodies. The expression of EF-Tu was detected by anti-EF-Tu antibodies as the loading control. *T*-test was used for statistical analyzes. Data are shown as means ± SEM; $n = 3$. $^*P < 0.05$, $^{**}P < 0.01$. Ery, erythromycin.

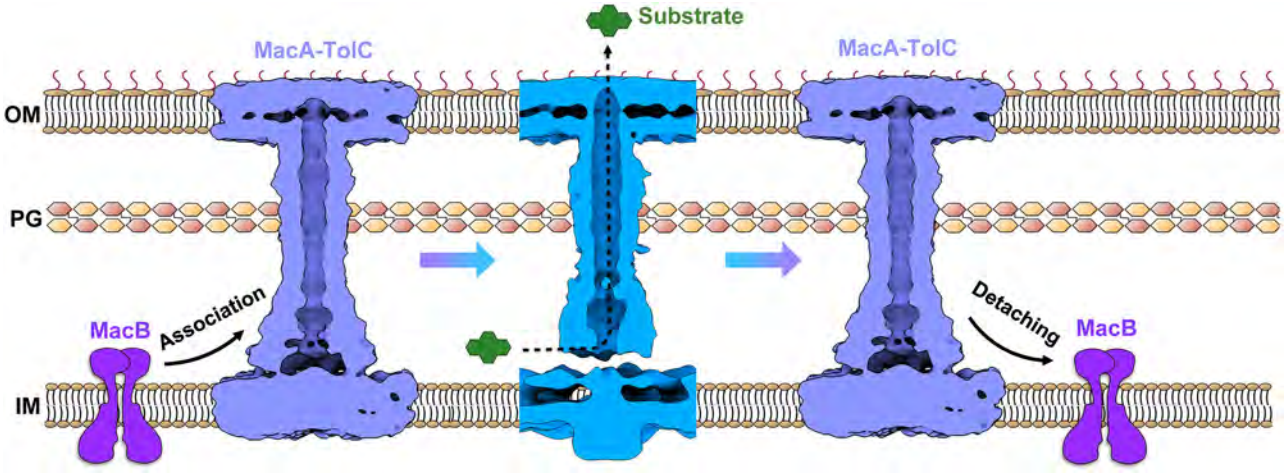

Fig. 4 | Proposed assembly and functioning mechanism of the ABC-type tripartite pump MacAB-TolC in *E.coli cells*. In the absence of substrates, MacA binds TolC to form the MacA-TolC subcomplex and then recruits MacB to assemble into the MacAB-TolC efflux pump. In the presence of substrates, MacAB-TolC hydrolyzes ATP to efflux substrates, and MacB dissociates from MacA-TolC subcomplex.

the absence of TolC, no MacA-MacB subcomplexes were observed across the cell envelope. Combining imaging results, protein crosslinking data, as well as previous works[10–13,19,20], we propose a model for the in situ assembly mechanism of MacAB-TolC (Fig. 4) (Supplementary Movie 1). Without substrates (apo state), MacA and TolC are likely to pre-form a bipartite complex for preparation of the accommodation of MacB. Next, MacB is recruited to form a stabilized tripartite MacAB-TolC pump. Upon the binding of the substrate to the pump, the MacB ATPase is triggered to be active, resulting in the hydrolysis of ATP and the expulsion of the substrates, followed by the subsequent dissociation of MacB from the full pump. Previous in vitro experiments suggested MacA-MacB binding in the absence of TolC[10,12,14], and MacA-TolC binding in the absence of MacB[10–13], however, we only observed MacA-TolC subcomplex inside *E. coli* cells. Similarly, in our previous in situ structure study of the AcrAB-TolC efflux pump, we observed only AcrA-AcrB subcomplexes but not AcrA-TolC subcomplexes[9], even though the biochemical data indicate that AcrA interacts with TolC without AcrB[13,21]. Under antibiotic pressure, the emergence of intermediate subcomplexes is quite surprising. The AcrAB-TolC efflux pump also presents this situation under antibiotic pressure[9]. Whether this phenomenon is common among tripartite efflux pumps remains unknown and the reason for it awaits further investigation.

Our results show that the MacAB-TolC pump is assembled in the near-to-native environment without antibiotic treatment. However, we cannot rule out the possibility that the assembly of the complex depends on the intracellular, yet unidentified substrate of MacAB-TolC efflux pump. It has been suggested that rough core lipopolysaccharide or a similar glycolipid and protoporphyrin are physiological substrates of MacAB-TolC[22,23].

Previous studies on MacB have shown that MacB exhibits two different conformations, ATP-bound or ADP-bound[6,7]. We are unable to determine whether MacB in our in situ structure was ATP-bound due to resolution limitations. However, we speculate that the MacB in the assembled MacAB-TolC in the near-to-native state is likely to be in an ATP-bound state, as in vitro experiments showed that ATP binding increased the affinity of the MacA-MacB complex, while ADP binding had a negative effect on MacAB interaction kinetics[10], and these affinity changes caused by ATP or ADP binding are likely to be more prominent in the real cell membrane environment. Additionally, it has been found that the binding of MacA to MacB stabilized the ATP-bound conformation of MacB in vitro[24]. Since ATP has been found to play a crucial role in the assembly process of the MacAB-TolC efflux pump[10,24], we speculate that the binding and hydrolysis of ATP might be among the intrinsic factors that trigger the association and dissociation of MacB with the MacA-TolC subcomplex. It has been found that without fusion or disulfide linkages of MacA and MacB, the fully assembled MacAB-TolC cannot be successfully purified[8], indicating that the interaction between MacA and MacB is sensitive to the lipid or bacterial cellular environment. It is likely that during the in vitro purification process, the degradation of ATP disrupts the binding of MacB to MacA-TolC subcomplex, which in turn leads to the failure of purifying the fully assembled MacAB-TolC. Furthermore, how MacB associates and dissociates from the MacA-TolC subcomplex without disassembly of the MacA hexamer awaits further studies.

Overall, our results suggest that the assembly sequence of MacAB-TolC is distinct from AcrAB-TolC, in which the AcrA-AcrB bipartite subcomplex forms first and TolC is recruited at the appropriate time[9]. It is conceivable that the assembly sequence of different tripartite pumps may not necessarily follow a similar manner, although TolC is required for the above two pumps to be functional. One of the possible reasons why MacAB-TolC and AcrAB-TolC present different assembly sequences in bacteria might be due to the difference in energizing mechanisms between ABC and RND transporters in the pumps.

These results present this distinct assembly process as a reference for designing novel efflux pump inhibitors. Confirming the MacA-TolC bipartite complex as a primary intermediate in the assembly process presents a novel target for therapeutic design. Given its unique occurrence in bacteria, targeting this crucial intermediate state during assembly can yield lower side effects in therapeutic interventions. This insight opens avenues for developing more precise and effective strategies in combating bacterial MDR.

Methods

Bacterial strains, plasmids, and protein expression

E. coli BW25113-Δ*acrB* strain was kindly provided by Dr. Xinmiao Fu at Fujian Normal University (Fuzhou, China). *E. coli* BL21 (DE3)-Δ*acrAB* strain was constructed by Ubigene Biosciences Co., Ltd (Guangzhou, China). The DNA sequences of *macAB* operon, *macA*, and *macB* (*E. coli* K12 strain) were synthesized by General Biosystems Co., Ltd (Anhui, China). It has been confirmed that adding a hexahistidine tag to the C-terminus of MacB does not affect the function of the MacAB-TolC efflux pump[8,10]. The *macAB* operon, *macA* gene, and *macB* gene, all with a C-terminal hexahistidine tag, were cloned into pBAD, yielding pBAD-*macAB*-his, pBAD-*macA*-his, and pBAD-*macB*-his, respectively. The *macA* gene with no tag was cloned into pETDuet, yielding pETDuet-*macA*. The pRSF-*tolC* plasmid was obtained from our previous study[9].

For cryo-ET imaging experiments, to overexpress the MacAB-TolC efflux pump, *E. coli* BL21 (DE3) cells were co-transformed with plasmids pBAD-*macAB*-his (ampicillin resistant) and pRSF-*tolC* (kanamycin

resistant). Cells were cultured at 37 °C in LB medium supplemented with 100 μg/ml ampicillin, 50 μg/ml kanamycin, and 0.02% L-arabinose to induce the expression of MacAB. When OD_{600} reached 0.8, 0.5 mM isopropyl 1-thio-β-D-galactopyranoside (IPTG) was added to induce the expression of TolC at 20 °C, 210 rpm overnight. To overexpress MacA and TolC, *E. coli* BL21 (DE3) cells were co-transformed with plasmids pETDuet-*macA* and pRSF-*tolC*. Cells were cultured at 37 °C in LB medium with 100 μg/ml ampicillin and 50 μg/ml kanamycin until an OD_{600} of 0.8 was reached, and protein expression was induced by adding 0.5 mM IPTG at 20 °C, 210 rpm overnight. To overexpress MacA and MacB, *E. coli* BW25113-Δ*tolC* cells were transformed with plasmids pBAD-*macAB*-his. Cells were cultured at 37 °C in LB medium with 100 μg/ml ampicillin and 50 μg/ml kanamycin until an OD_{600} of 0.8 was reached, and protein expression was induced by adding 0.02% L-arabinose at 20 °C, 210 rpm overnight.

Cryo-ET sample preparation

After induction, *E. coli* cells were harvested by centrifugation at 20,000 × *g* for 8 min, washed once with PBS buffer, and then centrifuged again at 20,000 × *g* for 8 min. Cells were then resuspended to an OD_{600} of 10. For cells expressing MacA and TolC, as well as those expressing MacA and MacB, these cells are ready for freezing in this step. For the erythromycin treatment state, cells expressing MacA, MacB, and TolC were added with 400 μg/ml erythromycin (equivalent to adding to an OD_{600} of 1 bacteria growth with 40 μg/ml erythromycin; the MIC of erythromycin for BL21 (DE3) cells overexpressing MacAB-TolC is 32 μg/ml) and incubated at 37 °C, 210 rpm for 30 min before freezing, while the near-to-native state cells were not treated by erythromycin. For freezing, cells were mixed with 6 nm BSA fiducial gold (Aurion, Wageningen, Netherlands) in a volume ratio of 3:1. A 3 μl droplet of the sample was applied to the freshly glow-discharged, continuous carbon film-covered grids (Quantifoil Cu R3.5/1, 200 mesh with 2 nm continuous carbon film, Quantifoil Micro Tools, Großlöbichau, Germany) and plunged frozen using a Vitrobot Mark IV (FEI, Oregon, USA). Grids were stored in liquid nitrogen until required for data collection.

Cryo-ET data collection and 3D reconstruction

The frozen-hydrated samples were imaged on a Titan Krios microscope with a Gatan K2 Summit direct electron detector camera. The magnification was 81,000×, with a pixel size of 1.76 Å. All tilt series were collected using a 3° angular step, from −51° to +51°, with a starting angle of −30°. The defocus ranges from −1.5 μm to −5 μm, and the total dose for each tilt series is about 100 $e^{-}/Å^{2}$.

Cryo-ET data processing

The raw frames were aligned using MotionCorr2[25]. For the near-to-native state MacAB-TolC dataset, 8734 particles were manually picked from 70 tomograms of good quality. Regarding every single particle, we manually picked it on the XY plane with its center Z position determined. After generating the initial model from scratch, 3D refinement was carried out using EMAN2[26–29]. The particle orientations from this refinement were visually examined using the evaluate refinement function in EMAN2, which maps the particles together with their orientations back to each tomogram, allowing an overview of the refinement quality. During this process, we observed that in some tomograms, most of the top-view particles are incorrectly aligned, hinting at an insufficient signal-to-noise ratio in these tomograms. Particles from these tomograms were excluded from the following data processing, leaving 5183 particles that were used for refinement from scratch again. Geometric features of the cell membrane were used to correct particle orientations[30]. To determine the symmetry of the in situ structure of MacAB-TolC, we first performed a C1 symmetry refinement and identified C3-symmetric features within the density map (Supplementary Fig. 11a, b). Based on these observations, we subsequently carried out refinement with C3 symmetry. Finally, a 14 Å density map was obtained, which could be fitted to the structure (PDB: 5NIK). The model fitting was carried out using the "Fit in Map" tool in UCSF Chimera. For details, the cryo-EM structure (PDB: 5NIK) was fitted into the map using the command "fitmap #1 #0 search 10 resolution 15 inside 0.6 metric correlation", which requires 10 hits with at least 60% of each hit inside the map contour. The best hit was chosen based on the highest correlation (>0.8).

For the dataset of MacAB-TolC under treatment of erythromycin, a similar process was conducted. An initial model was generated de novo using 877 manually picked particles from 68 good tomograms. After the initial model was built, one round of refinement using 2094 particles at a box size of 240 was performed, followed by a 3D classification using a mask focusing on the MacA MP domain. After classification, we noticed that one of the classes could be mixed with particles with MacB and without MacB, which cannot produce a converged model. However, the other class showed a higher resolution feature at the MacA MP domain. The converged model was refined from the combination of ~37% particles (772/2094) that did not have MacB density, and the ~35% particles (741/2094) that had very weak MacB density. We further refined the particles from this class by imposing C3 symmetry, based on the C3-symmetric features identified in the C1 refinement (Supplementary Fig. 11c, d), and a final model was obtained around 12 Å.

In this study, we assessed the quality of tomograms based on two main aspects: tilt series alignment accuracy and reconstructed tomogram quality. First, we visually examined each reconstructed tomogram in the dataset and evaluated the quality by observing the structural features in individual slices. A tomogram was classified as "good" when it met the following criteria: it clearly displayed key structural features such as the cell envelope (including membranes and cell wall) and visible pump-like particles, and had no obvious tilt image misalignment, no significant defocus off, and no loss of track of the image center. Only tomograms with these distinct and interpretable features were selected for subsequent analyzes.

As for the Fourier Shell Correlation (FSC) calculation, the FSC curve was automatically generated by using the e2spt_refine_new.py command in EMAN2 software to run the refinement. Following the gold standard of particle refinement, the FSC was calculated by comparing the even and odd maps after each iteration. We used the FSC file corresponding to the final iteration for 3D refinement. To verify the orientation of the aligned particles, we used the "Map particles to tomograms" function in EMAN2 and observed that most particles on the cell envelope were oriented as expected, with their axes approximately perpendicular to the cell envelope (Supplementary Fig. 12).

MIC assay

MIC of erythromycin was determined by a two-fold method according to Tikhonova et al.[31], with minor modifications. Briefly, exponentially growing *E. coli* cultures (OD_{600} of 0.8) were inoculated at a density of 10^4 cells per ml into an LB medium containing protein expression inducers and appropriate antibiotics in the presence of serial twofold increasing concentrations of erythromycin. Cell growth was determined visually after incubation at 37 °C for 20 h. For the *E. coli* BW25113-Δ*acrB* cells expressing Bpa variants, cultures were inoculated at a density of 10^6 cells per ml, as the solvent sodium hydroxide used for dissolving Bpa is toxic to bacteria. All MIC measurements were repeated five times.

In vivo site-specific photo-crosslinking mediated by photo-reactive amino acid Bpa

For Bpa-mediated in vivo photo-crosslinking experiments, plasmids for expressing Bpa variants of MacA and MacB were generated from the template plasmids pBAD-*macAB*-his/pBAD-*macB*-his/pBAD-*macA*-his using the QuickChange site-directed mutagenesis kit (Transgene, Beijing, China). The pSup-BpaRS6TRN plasmid (chloramphenicol resistant, preserved in our lab), which expresses the orthogonal aminoacyl-tRNA synthetase/tRNA pair for the incorporation of Bpa into the protein of interest, was co-transformed with pBAD-*macAB*-his/pBAD-*macB*-his/pBAD-*macA*-his carrying mutations at the target sites and pRSF-*tolC* into *E. coli* BL21 (DE3) cells. Cells were cultured in the presence of 100 μg/ml ampicillin, 50 μg/ml kanamycin, 50 μg/ml chloramphenicol, 1 mM Bpa

(Macklin, Shanghai, China), and 0.02% L-arabinose and 0.1 mM IPTG to induce protein expression.

To investigate the effect of erythromycin on MacA-MacB interaction, *E. coli* cells were first adjusted to an OD_{600} of 1. After that, 40 μg/ml erythromycin was added and cells were incubated at 37 °C, 210 rpm for 30 min. Cells without erythromycin treatment were incubated under the same conditions as the control. For the photo-crosslinking reaction, *E. coli* cells were transferred to a 6-well plate (on ice), followed by UV irradiation at 365 nm for indicated time using an ultraviolet cross-linker (Scientz, Ningbo, China). The cells were then lysed with SDS sample loading buffer before being analyzed by SDS-PAGE and immunoblotting with anti-his tag monoclonal antibodies (1:1000; Cat# HRP-66005, Proteintech, Chicago, USA) and anti-EF-Tu monoclonal antibodies (1: 10,000, preserved in our lab). Protein bands were visualized with an ECL detection system (Beyotime Institute of Biotechnology, Shanghai, China) and quantified densitometrically with ImageJ software.

Quantification of the photo-crosslinked MacA-MacB product

The relative level of the photo-crosslinked MacA-MacB was calculated based on the immunoblot results. First, a densitometric analysis of the immunoblots was conducted using the NIH ImageJ program. Then, to obtain a reliable relative value, the intensity of the cross-linked MacA-MacB was divided by that of the MacB monomer, and further divided by the intensity of the loading control EF-Tu. Finally, to make the data more manageable and easier to present, the resulting value was multiplied by 10,000.

Statistics and reproducibility

All the MIC assays were independently repeated five times for the tested *E. coli* strains. The MIC data were analyzed by Mann–Whitney test or one-way ANOVA, followed by Tukey's multiple comparisons test. The NIH ImageJ program was used to conduct a densitometric analysis of the immunoblots. For the relative MacB level and the relative photo-crosslinked MacA-MacB analysis, each experiment was independently repeated three times, and *t*-test was used to assess differences. GraphPad Prism 9.0 was used for data analysis. $P < 0.05$ was considered statistically significant. Data were presented as means ± SEM. For the expression analysis of MacA/MacB Bpa variants, all immunoblotting results were obtained from three independent experimental replicates with consistent results.

Reporting summary

Further information on research design is available in the Nature Portfolio Reporting Summary linked to this article.

Data availability

The authors declare that the data supporting the findings of this study are available from the corresponding authors W.Z., and X.S., upon request. Source data related to the graphs and charts in this paper are provided in Supplementary Data 1–4. Tomographic reconstruction data that support the findings of this study have been deposited in EMDB with the accession codes EMD-44384 (near-to-native state) and EMD-44385 (erythromycin-present state). Uncropped and unedited blot/gel images are provided in the Supplementary Information PDF. Statistics of in situ structures achieved in this study are provided in the Supplementary Table 3.

Code availability

All the relevant codes are available in the EMAN2 package.

Received: 11 November 2024; Accepted: 15 May 2025;
Published online: 03 June 2025

References

1. Du, D., van Veen, H. W. & Luisi, B. F. Assembly and operation of bacterial tripartite multidrug efflux pumps. *Trends Microbiol.* **23**, 311–319 (2015).
2. Kobayashi, N., Nishino, K. & Yamaguchi, A. Novel macrolide-specific ABC-type efflux transporter in Escherichia coli. *J. Bacteriol.* **183**, 5639–5644 (2001).
3. Greene, N. P., Kaplan, E., Crow, A. & Koronakis, V. Antibiotic resistance mediated by the MacB ABC transporter family: a structural and functional perspective. *Front. Microbiol.* **9**, 950 (2018).
4. Yum, S. et al. Crystal structure of the periplasmic component of a tripartite macrolide-specific efflux pump. *J. Mol. Biol.* **387**, 1286–1297 (2009).
5. Koronakis, V., Sharff, A., Koronakis, E., Luisi, B. & Hughes, C. Crystal structure of the bacterial membrane protein TolC central to multidrug efflux and protein export. *Nature* **405**, 914–919 (2000).
6. Crow, A., Greene, N. P., Kaplan, E. & Koronakis, V. Structure and mechanotransmission mechanism of the MacB ABC transporter superfamily. *Proc. Natl. Acad. Sci. USA* **114**, 12572–12577 (2017).
7. Okada, U. et al. Crystal structure of tripartite-type ABC transporter MacB from Acinetobacter baumannii. *Nat. Commun.* **8**, 1336 (2017).
8. Fitzpatrick, A. W. P. et al. Structure of the MacAB-TolC ABC-type tripartite multidrug efflux pump. *Nat. Microbiol.* **2**, 17070 (2017).
9. Shi, X. et al. In situ structure and assembly of the multidrug efflux pump AcrAB-TolC. *Nat. Commun.* **10**, 2635 (2019).
10. Lu, S. & Zgurskaya, H. I. Role of ATP binding and hydrolysis in assembly of MacAB-TolC macrolide transporter. *Mol. Microbiol.* **86**, 1132–1143 (2012).
11. Xu, Y. et al. Functional implications of an intermeshing cogwheel-like interaction between TolC and MacA in the action of macrolide-specific efflux pump MacAB-TolC. *J. Biol. Chem.* **286**, 13541–13549 (2011).
12. Lin, H. T. et al. MacB ABC transporter is a dimer whose ATPase activity and macrolide-binding capacity are regulated by the membrane fusion protein MacA. *J. Biol. Chem.* **284**, 1145–1154 (2009).
13. Tikhonova, E. B., Dastidar, V., Rybenkov, V. V. & Zgurskaya, H. I. Kinetic control of TolC recruitment by multidrug efflux complexes. *Proc. Natl. Acad. Sci. USA* **106**, 16416–16421 (2009).
14. Tikhonova, E. B., Devroy, V. K., Lau, S. Y. & Zgurskaya, H. I. Reconstitution of the Escherichia coli macrolide transporter: the periplasmic membrane fusion protein MacA stimulates the ATPase activity of MacB. *Mol. Microbiol.* **63**, 895–910 (2007).
15. Chen, M. et al. In situ structure of the AcrAB-TolC efflux pump at subnanometer resolution. *Structure* **30**, 107–113.e103 (2022).
16. Tang, L. et al. Occurrence, distribution, and behaviors of erythromycin A, production byproducts, transformation products, and resistance genes in a full-scale erythromycin A production wastewater treatment system. *Water Res.* **245**, 120640 (2023).
17. Tao, K., Narita, S. I., Okada, U., Murakami, S. & Tokuda, H. Dissection of an ABC transporter LolCDE function analyzed by photo-crosslinking. *J. Biochem.* **175**, 427–437 (2024).
18. Agirre, J. et al. The CCP4 suite: integrative software for macromolecular crystallography. *Acta Crystallogr. D Struct. Biol.* **79**, 449–461 (2023).
19. Batista Dos Santos, W., Souabni, H. & Picard, M. Corseting a tripartite ABC transporter to make it fit for transport. *Biochimie* **205**, 117–123 (2023).
20. Souabni, H. et al. Quantitative real-time analysis of the efflux by the MacAB-TolC tripartite efflux pump clarifies the role of ATP hydrolysis within mechanotransmission mechanism. *Commun. Biol.* **4**, 493 (2021).
21. Touze, T. et al. Interactions underlying assembly of the Escherichia coli AcrAB-TolC multidrug efflux system. *Mol. Microbiol.* **53**, 697–706 (2004).
22. Lu, S. & Zgurskaya, H. I. MacA, a periplasmic membrane fusion protein of the macrolide transporter MacAB-TolC, binds lipopolysaccharide core specifically and with high affinity. *J. Bacteriol.* **195**, 4865–4872 (2013).

23. Turlin, E. et al. Protoporphyrin (PPIX) efflux by the MacAB-TolC pump in Escherichia coli. *Microbiologyopen* **3**, 849–859 (2014).
24. Modali, S. D. & Zgurskaya, H. I. The periplasmic membrane proximal domain of MacA acts as a switch in stimulation of ATP hydrolysis by MacB transporter. *Mol. Microbiol.* **81**, 937–951 (2011).
25. Zheng, S. Q. et al. MotionCor2: anisotropic correction of beam-induced motion for improved cryo-electron microscopy. *Nat. Methods* **14**, 331–332 (2017).
26. Tang, G. et al. EMAN2: an extensible image processing suite for electron microscopy. *J. Struct. Biol.* **157**, 38–46 (2007).
27. Ludtke, S. J. Single-particle refinement and variability analysis in EMAN2.1. *Methods Enzymol.* **579**, 159–189 (2016).
28. Chen, M. et al. Convolutional neural networks for automated annotation of cellular cryo-electron tomograms. *Nat. Methods* **14**, 983–985 (2017).
29. Chen, M. et al. A complete data processing workflow for cryo-ET and subtomogram averaging. *Nat. Methods* **16**, 1161–1168 (2019).
30. Yu, Z. et al. Membrane translocation process revealed by in situ structures of type II secretion system secretins. *Nat. Commun.* **14**, 4025 (2023).
31. Tikhonova, E. B., Wang, Q. & Zgurskaya, H. I. Chimeric analysis of the multicomponent multidrug efflux transporters from gram-negative bacteria. *J. Bacteriol.* **184**, 6499–6507 (2002).

Acknowledgements

This work was supported by R01AI179879, R01HL162842, and Welch Foundation Q-2173-20230405 funds to Z.W.; the National Natural Science Foundation of China (No. 82072312), and the Natural Science Foundation of Jiangsu Province (No. BK20211053) to X.S.; the State Key Program of National Natural Science Foundation of China (82130033) to J.C.; Post-graduate Research & Practice Innovation Program of Jiangsu Province (No. KYCX22_2925, KYCX23_2958, and KYCX24_3131). Cryo-EM data were collected at the Baylor College of Medicine Cryo-EM ATC and UTHealth Cryo-EM Core, which includes equipment purchased under the support of CPRIT Core Facility Award RP190602. We thank Dr. Dijun Du, who is currently working at the ShanghaiTech University in China, and Dr. Ben Luisi from the University of Cambridge in the UK for sharing the plasmid vector pRSF-*tolC*. We thank Valerie Dalton for revising the paper language and Snekalatha Raveendran for data backup.

Author contributions

Xiaodong Shi, Zhao Wang, and Tong Huo designed experiments. Zhili Yu and Xiaodong Shi performed sample freezing and cryo-ET imaging. Tong Huo and Zhili Yu did cryo-ET data processing. Wenfang Zhang, Wei Zheng, Yaoming Wu, Qiuyu Ren, and Zekai Wan performed biochemistry experiments. Xiaodong Shi and Tong Huo wrote the initial manuscript. Zhao Wang, Junli Cao, and Zhili Yu revised the manuscript.

Competing interests

The authors declare no competing interests.

Additional information

Supplementary information The online version contains supplementary material available at https://doi.org/10.1038/s42003-025-08236-z.

Correspondence and requests for materials should be addressed to Junli Cao, Zhao Wang or Xiaodong Shi.

Peer review information *Communications Biology* thanks the anonymous reviewers for their contribution to the peer review of this work. Primary Handling Editors: Antonio Calabrese and Aylin Bircan.